Helicity statistics in homogeneous and isotropic turbulence and turbulence models

Ganapati Sahoo, Massimo De Pietro, and Luca Biferale
*Department of Physics & INFN, University of Rome Tor Vergata, Via della Ricerca Scientifica 1,
00133 Rome, Italy*

We study the statistical properties of helicity in direct numerical simulations of fully developed homogeneous and isotropic turbulence and in a class of turbulence shell models. We consider correlation functions based on combinations of vorticity and velocity increments that are not invariant under mirror symmetry. We also study the scaling properties of high-order structure functions based on the moments of the velocity increments projected on a subset of modes with either positive or negative helicity (chirality). We show that mirror symmetry is recovered at small scales, i.e., chiral terms are subleading and they are well captured by a dimensional argument plus anomalous corrections. These findings are also supported by a high Reynolds numbers study of helical shell models with the same chiral symmetry of Navier-Stokes equations.

I. INTRODUCTION

All phenomenological theories of three-dimensional (3D) turbulence are based on the concept of direct energy cascade [1]. However, helicity is also an inviscid invariant of the 3D Navier-Stokes equations (NSEs) defined as the scalar product of velocity $\boldsymbol{u}(\boldsymbol{x})$ with vorticity $\boldsymbol{\omega}(\boldsymbol{x})$. Its mean value

$$H = \frac{1}{V} \int_V d^3x \, \boldsymbol{u}(\boldsymbol{x}) \cdot \boldsymbol{\omega}(\boldsymbol{x}) \tag{1}$$

is exactly zero if the flow is invariant under mirror symmetry, $\boldsymbol{\omega}$ being a pseudovector. Since its discovery [2–4], helicity has been the object of many speculations. In particular, it is not clear if the presence of a nonzero mean helicity, globally or locally, can affect the statistical properties of the forward energy cascade. On the one hand, because the nonlinear term of the NSE is locally proportional to the solenoidal component of $\boldsymbol{u} \times \boldsymbol{\omega}$, flows with a nonzero helicity might have a strongly depleted energy transfer [5,6]. On the other hand, helicity is not sign-definite, and therefore cancellations might eventually smooth down this *blocking* mechanism [7,8]. There exist instances where helicity plays a key role, interfering with the energy transfer, as in rotating turbulence [9,10], in shear flows [11], and in the case of an NSE confined to evolve on a subset of sign-definite helical modes [12–15]. In the presence of a stationary helicity injection, we have an exact law which predicts the scaling properties of a specific velocity-vorticity mixed third-order correlation function [16–18]. Nevertheless, this is not a strong constraint for the whole statistics. Indeed, different phenomenological scaling for the spectral properties has been proposed in the presence of two simultaneous fluxes of energy and helicity [4,7,19].

In this paper we further investigate the statistical properties of helicity in fully developed turbulence by using high-resolution direct numerical simulations (DNSs). In order to have a proper way to distinguish the importance of mirror-symmetry-breaking contributions *scale-by-scale*, we study the properties of a class of structure functions based on velocity increments decomposed on positive or negative helical modes. The latter have the advantage of observable definitions that are sensitive to lack of mirror symmetry for all moments, odd or even, differently from what was proposed earlier in Refs. [8,20]. Furthermore, we also introduce a set of velocity-vorticity correlation functions based on the helicity cancellation exponent [21] that allows us to quantify the breaking of mirror symmetry also on quantities based on velocity gradients.

We show that helicity-sensitive observables are always subleading with respect to the ones dominated by the energy flux. Results are also supported by studying analogous quantities in a helical shell model [7,22,23]. We show that the scaling behavior of chiral quantities is well captured by an analytical contribution in terms of the helicity flux, plus a small anomalous correction.

II. PHENOMENOLOGICAL BACKGROUND

We consider the 3D forced NSE

$$\partial_t \boldsymbol{u} + \boldsymbol{u} \cdot \nabla \boldsymbol{u} = -\nabla p + \nu \Delta \boldsymbol{u} + \boldsymbol{f}, \tag{2}$$

where p is the pressure, ν is the kinematic viscosity, and $\boldsymbol{f}$ is a parity-breaking external forcing mechanism with energy injection $\varepsilon = \langle \boldsymbol{u} \cdot \boldsymbol{f} \rangle$ and helicity injection $h = \langle \boldsymbol{u} \cdot (\nabla \times \boldsymbol{f}) + \boldsymbol{\omega} \cdot \boldsymbol{f} \rangle$. Under the assumptions of stationarity, homogeneity, and isotropy (but not mirror symmetry) it is possible to derive two exact equations for two-point third-order correlation functions [1,16,17,24]:

$$\langle (\delta_r u)^3 \rangle = -\tfrac{4}{5}\varepsilon\, r, \tag{3}$$

$$\langle \delta_r u (\delta_r \boldsymbol{u} \cdot \delta_r \boldsymbol{\omega}) \rangle - \tfrac{1}{2} \langle \delta_r \omega (\delta_r \boldsymbol{u} \cdot \delta_r \boldsymbol{u}) \rangle = -\tfrac{4}{3} h\, r, \tag{4}$$

where $\delta_r u$ and $\delta_r \omega$ are, respectively, the longitudinal velocity and vorticity increments, defined in terms of the projection on the unit vector $\hat{\boldsymbol{r}}$: $\delta_r X = \delta_r X \cdot \hat{\boldsymbol{r}}$, and the generic vector increment between two points is $\delta_r X = X(r + x) - X(x)$. Notice that (4) is different from zero only in the presence of a mirror-breaking forcing mechanism. The two exact scaling relations (3) and (4) are valid in the inertial range, i.e., when the increment r is chosen in a range of scales where dissipative and forcing effects can be neglected. Moreover, since helicity is not sign-definite, it is not possible to predict the energy transfer direction: both a simultaneous cascade of energy and helicity toward small scales and a split cascade with energy flowing upward and helicity downward are possible [4,11,13,25]. In order to disentangle in a systematic way the statistical properties under mirror symmetry, it is useful to adopt an exact decomposition of the velocity field in positive and negative Fourier helical waves [26,27]:

$$\boldsymbol{u}(\boldsymbol{x},t) = \sum_{\boldsymbol{k}} [u_{\boldsymbol{k}}^+(t) \boldsymbol{h}_{\boldsymbol{k}}^+ + u_{\boldsymbol{k}}^-(t) \boldsymbol{h}_{\boldsymbol{k}}^-] \mathrm{e}^{i\boldsymbol{k}\cdot\boldsymbol{x}}, \tag{5}$$

where $\boldsymbol{h}_{\boldsymbol{k}}^{\pm}$ are the eigenvectors of the curl, i.e., $i\boldsymbol{k} \times \boldsymbol{h}_{\boldsymbol{k}}^{\pm} = \pm k \boldsymbol{h}_{\boldsymbol{k}}^{\pm}$. We choose $\boldsymbol{h}_{\boldsymbol{k}}^{\pm} = \hat{\mu}_{\boldsymbol{k}} \times \hat{k} \pm i \hat{\mu}_{\boldsymbol{k}}$, where $\hat{\mu}_{\boldsymbol{k}}$ is a unit vector orthogonal to $\boldsymbol{k}$ satisfying the condition $\hat{\mu}_{\boldsymbol{k}} = -\hat{\mu}_{-\boldsymbol{k}}$, e.g., $\hat{\mu}_{\boldsymbol{k}} = \boldsymbol{z} \times \boldsymbol{k} / ||\boldsymbol{z} \times \boldsymbol{k}||$, with any arbitrary vector $\boldsymbol{z}$. In terms of such decomposition the total energy, $E = \int d^3x\, |\boldsymbol{u}(\boldsymbol{x})|^2$, and the total helicity are written as

$$E = \sum_{\boldsymbol{k}} |u_{\boldsymbol{k}}^+|^2 + |u_{\boldsymbol{k}}^-|^2, \tag{6}$$

$$H = \sum_{\boldsymbol{k}} k\,(|u_{\boldsymbol{k}}^+|^2 - |u_{\boldsymbol{k}}^-|^2). \tag{7}$$

It is useful to further distinguish the energy content of the positive and negative helical modes, $E^{\pm}(k) = \sum_{k \leqslant |\boldsymbol{k}| < k+1} |u_{\boldsymbol{k}}^{\pm}|^2$, such that we have for the energy and helicity spectra [7]

$$E(k) = E^+(k) + E^-(k), \tag{8}$$

$$H(k) = k\,[E^+(k) - E^-(k)]. \tag{9}$$

It is straightforward to realize that the equivalent of (8) and (9) in real space is given by the second-order correlation functions decomposed in terms of the fields $\boldsymbol{u}^{\pm}(\boldsymbol{x}) = \sum_{\boldsymbol{k}} u_{\boldsymbol{k}}^{\pm}(t) \boldsymbol{h}_{\boldsymbol{k}}^{\pm} \exp^{i\boldsymbol{k}\cdot\boldsymbol{x}}$:

$$\langle \delta_r u_i \delta_r u_i \rangle = \langle \delta_r u_i^+ \delta_r u_i^+ \rangle + \langle \delta_r u_i^- \delta_r u_i^- \rangle, \tag{10}$$

$$\langle \delta_r u_i \delta_r \omega_i \rangle = \langle \delta_r u_i^+ \delta_r \omega_i^+ \rangle + \langle \delta_r u_i^- \delta_r \omega_i^- \rangle, \tag{11}$$

because both mixed terms $\langle \delta_r u_i^\pm \delta_r \omega_i^\mp \rangle$ and $\langle \delta_r u_i^\pm \delta_r u_i^\mp \rangle$ vanish, due to the orthonormality of $\boldsymbol{h}_{\boldsymbol{k}}^\pm$.

It is not possible to derive a closed expression for the energy and helicity spectra from (3) and (4) alone, because there exists a continuum of possible combinations of ε, h, and k with the correct dimensional properties:

$$E(k) = \varepsilon^{\frac{2}{3} - \alpha} h^\alpha k^{-\frac{5}{3} - \alpha}. \tag{12}$$

Different possibilities have been proposed, based on different closures of the spectral equations, depending on the dynamical time scale that drives the energy and helicity transfers. One possibility is based on the idea that the only relevant time scale is the one given by the energy fluctuations, $\tau_r^E \sim \varepsilon^{-1/3} r^{2/3}$. In this case we have the dimensional estimate for the (mirror invariant) energy flux:

$$\varepsilon \sim \langle \delta_r u_i \delta_r u_i \rangle / \tau_r^E \rightarrow \langle (\delta_r u)^2 \rangle \sim \varepsilon^{2/3} r^{2/3}, \tag{13}$$

while for the chiral term,

$$h \sim \langle \delta_r u_i \delta_r \omega_i \rangle / \tau_r^E \rightarrow \langle \delta_r u_i \delta_r \omega_i \rangle \sim h \varepsilon^{-1/3} r^{2/3}. \tag{14}$$

Translating back to Fourier space we would then have for the semisum (mirror-symmetric) and the semidifference (mirror-antisymmetric) of the spectral components [7]:

$$E^+(k) + E^-(k) \sim C_E \varepsilon^{2/3} k^{-5/3}, \tag{15}$$

$$E^+(k) - E^-(k) \sim C_H h \varepsilon^{-1/3} k^{-8/3}, \tag{16}$$

where C_E and C_H are two dimensionless constants. Hence, the two energy components can be written as

$$E^\pm(k) \sim C_E \varepsilon^{2/3} k^{-5/3} \pm C_H h \varepsilon^{-1/3} k^{-8/3}. \tag{17}$$

Another possible dimensional closure employs the helicity time scale, $\tau_r^H \sim h^{-1/3} r^{1/3}$, to evaluate both fluxes (13) and (14). In this case we have [19]

$$E^\pm(k) \sim C_E \varepsilon h^{-1/3} k^{-4/3} \pm C_H h^{2/3} k^{-7/3}. \tag{18}$$

Relation (18) breaks the $-5/3$ law for the energy spectrum and has been proposed to be valid only in the high-k region of strongly helical turbulence, to explain the bottleneck observed close to the viscous scale. Indeed, relation (18) is not smooth for $h \rightarrow 0$ and therefore cannot be considered a good option if helicity is subleading. A third possible scenario is a split cascade, where energy flows upward and helicity downward. In this case, in the forward-helicity cascade range, only h flux appears, and the dimensional prediction gives

$$E(k) \sim h^{2/3} k^{-7/3}, \quad H(k) \sim h^{2/3} k^{-4/3}. \tag{19}$$

This last scenario has never been observed in isotropic turbulence, unless a dynamical mode reduction on helical modes with the same sign is imposed [12,13,27]. Besides the open issues concerning the spectral properties and higher-order statistics are even less studied and understood. There are very few measurements of the mirror-antisymmetric components of structure functions. As a result, while a huge amount of work has been devoted to intermittency and anomalous scaling properties of the mirror-symmetric components, very little is known about the helical components [8,20]. In what follows we will investigate further the statistical properties of helical turbulence concerning its spectral properties and beyond, assessing also the chiral components of high-order correlation functions. In particular, we will study the scaling properties of longitudinal structure functions based only on positive or negative helical modes:

$$S_p^\pm(r) = \langle (\delta_r u^\pm)^p \rangle. \tag{20}$$

TABLE I. Details of the simulations. N: number of collocation points along each axis; L: size of the periodic box; ν: kinematic viscosity; k_f: range of forced wave numbers; u_{rms}: rms velocity; $Re_\lambda = u_{rms}\lambda/\nu$: Taylor-microscale Reynolds number, where $\lambda = \frac{2\pi}{L}\sqrt{\frac{\langle u^2(x)\rangle}{\langle[\partial_x u(x)]^2\rangle}}$ is the Taylor microscale; ε: mean energy dissipation rate; η: Kolmogorov length scale; T_0: large-eddy-turnover time.

Run	N	L	ν	k_f	u_{rms}	Re_λ	ε	η	T_0
R1	1024	2π	0.001	[1,2]	3.4	320	3.2	0.004	0.3

In terms of the above decomposition, we can define energy- or helicity-like structure functions, i.e., combinations that are symmetric or antisymmetric for the exchange of positive and negative helical projections:

$$S_p^E(r) = \langle(\delta_r u^+)^p\rangle + \langle(\delta_r u^-)^p\rangle \sim r^{\zeta_p^E}, \tag{21}$$

$$S_p^H(r) = \langle(\delta_r u^+)^p\rangle - \langle(\delta_r u^-)^p\rangle \sim r^{\zeta_p^H}. \tag{22}$$

The advantage of working with the above definition is to avoid observables based on vorticity increments, which are strongly influenced by viscous contributions and might not have a power law scaling in the inertial range. In order to have a dimensional estimate for (21) and (22) we start from the phenomenological predictions (17) considering the helical component to be subleading. Then one might dimensionally write

$$\delta_r u^\pm \sim \varepsilon^{1/3} r^{1/3} \pm h\varepsilon^{-2/3} r^{4/3}, \tag{23}$$

and therefore conclude that, at the lowest order in h,

$$S_p^E(r) \sim \varepsilon^{\frac{p}{3}} r^{\frac{p}{3}} + o(h), \tag{24}$$

$$S_p^H(r) \sim \varepsilon^{\frac{p}{3}-1} h r^{\frac{p}{3}+1} + O(h^2), \tag{25}$$

where the second relation is obtained taking into account that the leading terms proportional to $\varepsilon^{p/3}$ cancel out.

Another possible way to highlight the scaling properties of the helical component of the *scale-by-scale* velocity statistics is to look directly at the local helicity increments:

$$\mathcal{H}_p(r) = \langle \text{sign}(\delta_r u_i \delta_r \omega_i)|\delta_r u_i \delta_r \omega_i|^p\rangle, \tag{26}$$

where we have introduced the sign function in order to have a chiral observable for all orders of the moment p [28,29]. The mean value of the *sign* of local helicity, which gives a direct measure of the
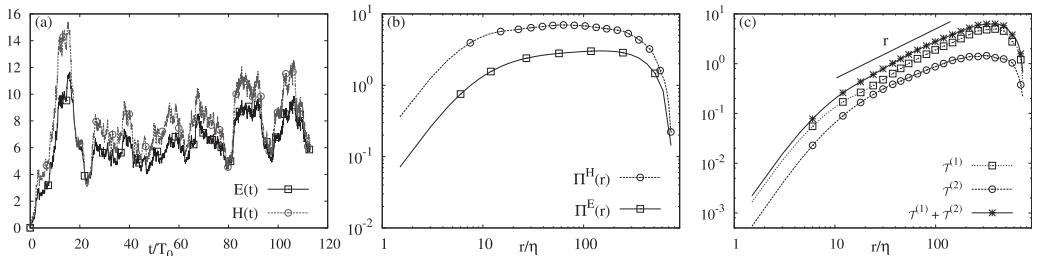

FIG. 1. (a) Temporal evolution of total energy and helicity from DNS with injection of helicity (R1). (b) Flux of energy $\Pi^E(r) = \langle(\delta_r u)^3\rangle/r$ and flux of helicity $\Pi^H(r) = [\mathcal{T}^{(1)} + \mathcal{T}^{(2)}]/r$, in real space, where $\mathcal{T}^{(1)} = \langle\delta_r u(\delta_r \boldsymbol{u} \cdot \delta_r \boldsymbol{\omega})\rangle$ and $\mathcal{T}^{(2)} = -0.5\langle\delta_r \omega(\delta_r \boldsymbol{u} \cdot \delta_r \boldsymbol{u})\rangle$ [see Eqs. (3) and (4)]. (c) Scaling of the first term $\mathcal{T}^{(1)}$, the second term $\mathcal{T}^{(2)}$, and their sum in (4). The solid line is drawn with slope 1 for comparison.

relative importance of chiral fluctuations with respect to the nonchiral background, is known as the *cancellation exponent* [21] and can be estimated dimensionally to be

$$\mathcal{H}_0(r) = \left\langle \frac{\delta_r u_i \delta_r \omega_i}{|\delta_r u_i \delta_r \omega_i|} \right\rangle \sim \frac{h \varepsilon^{-1/3} r^{2/3}}{\varepsilon^{2/3} r^{1/3} \eta^{-2/3}} \sim h \varepsilon^{-1} r^{1/3} \eta^{2/3}, \tag{27}$$

where we write the numerator in terms of its dominant helical contribution and the denominator as the mirror-symmetric term with $|\delta_r u| \sim \varepsilon^{1/3} r^{1/3}$ and $|\delta_r \omega| \sim \varepsilon^{1/3} \eta^{-2/3}$. Here η is the Kolmogorov length scale, where the vorticity increment is expected to be maximal. As a result, we should have for (26) the scaling property:

$$\mathcal{H}_p(r) \sim h \eta^{\frac{2-2p}{3}} \varepsilon^{\frac{2p-3}{3}} r^{\frac{p+1}{3}}. \tag{28}$$

III. NUMERICAL SIMULATIONS OF NAVIER-STOKES EQUATIONS

We have performed a series of DNSs of the NSE (2) with a fully dealiased, pseudospectral code at a resolution of 1024^3 collocation points on a triply periodic cubic domain of size $L = 2\pi$. The flow is sustained by a random Gaussian forcing with

$$\langle f_i(\boldsymbol{k},t) f_j(\boldsymbol{q},t') \rangle = F(k)\delta(\boldsymbol{k} - \boldsymbol{q})\delta(t - t')Q_{i,j}(\boldsymbol{k}),$$
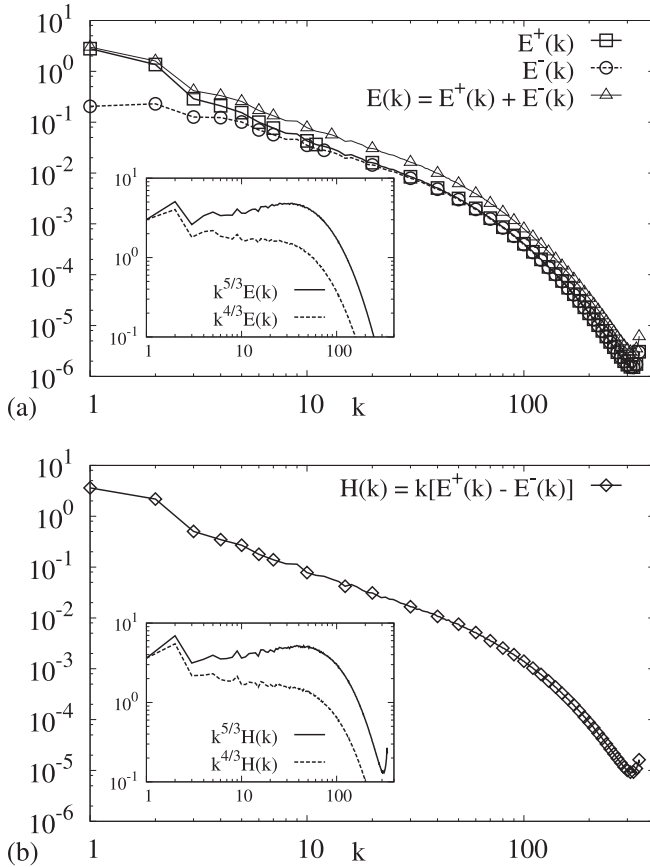

FIG. 2. (a) Log-log plots of energy spectrum $E(k)$ and its helical components $E^{\pm}(k)$. Inset: Compensated energy spectra with predictions (17) and (18). (b) Log-log plots of helicity spectrum $H(k)$. Inset: Compensated helicity spectra with predictions (17) and (18).
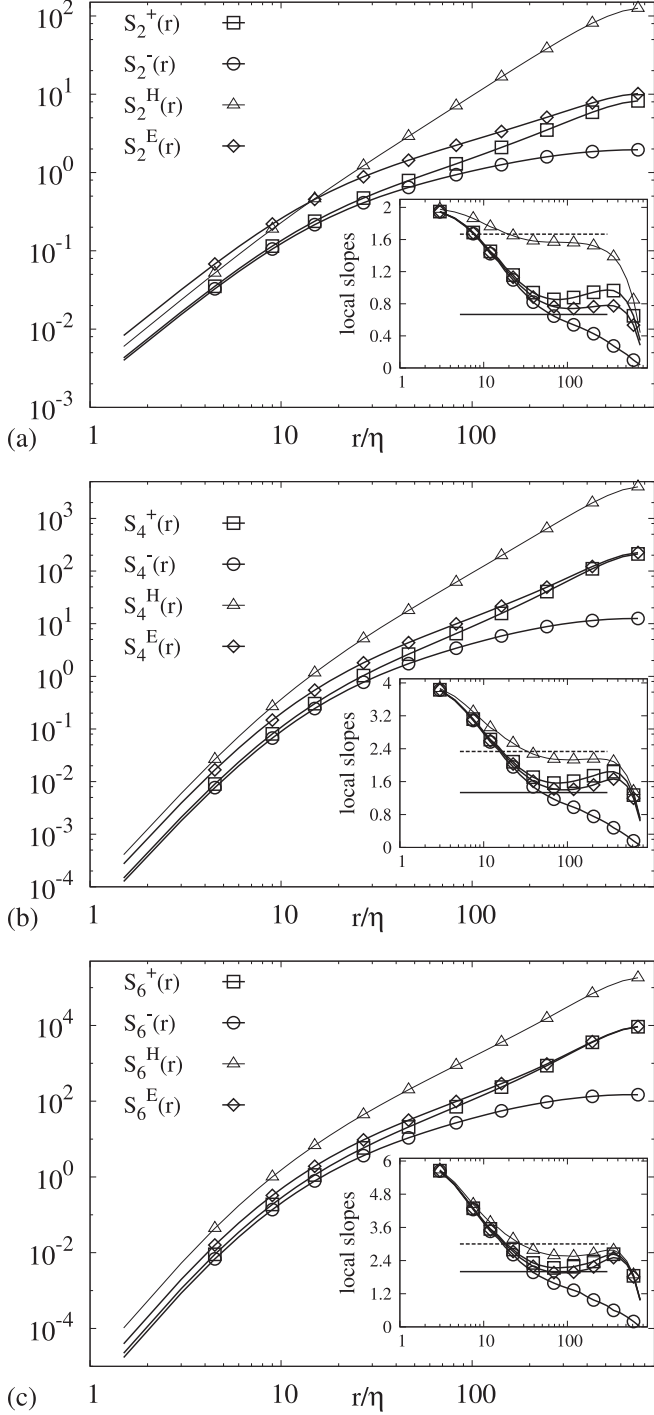
FIG. 3. Log-log plots of structure functions in real space for (a) second, (b) fourth, and (c) sixth order based on positive or negative, $S_p^{\pm}(r)$, helical modes and their combinations, $S_p^{E,H}(r)$. $S_p^H(r)$ are multiplied with a scalar factor for better representation. Inset: Local slopes of the curves showing $\zeta_p^{E,H}(r)$ and $\zeta_p^{\pm}(r)$ [see (29)]. Dimensional predictions (solid lines for $p/3$ and dashed lines for $\frac{p}{3}+1$) are also shown for comparison, where p is the order of the structure functions.

where $Q_{ij}(\boldsymbol{k})$ is a projector imposing incompressibility and $F(k)$ has support only for $k_f \in [k_{\min}, k_{\max}]$. We carried out a DNS, namely, R1, where we inject maximal helicity by forcing only the positive helical modes of the velocity (see Table I).

In Fig. 1(a) we show the evolution of the total energy E and helicity H and of their fluxes in real space [Fig. 1(b)]. It is clear that the system is in a stationary state with a dual forward cascade of energy and helicity. Figure 1(c) shows that the two contributions entering in (4) have different properties in the inertial range and that only their sum shows a good linear behavior as predicted by the constant-helicity-flux solution. This is not surprising; we must expect that in the presence of two transferred quantities only particular combinations of correlation functions might have an exact scaling behavior, while any general combination of fields might be affected by leading and subleading contributions.

In Fig. 2 we show the energy and helicity spectra and their positive and negative helical components $E^{\pm}(k)$. We observe that the predictions (15) and (16) give a better compensation at least for not too high wave numbers where a dissipative bottleneck is known to affect the local scaling properties. At those wave numbers, the relative helicity $H(k)/kE(k)$ is already very small, and it is unlikely that the bottleneck is due to some helical effects as proposed by (18). Concerning real-space quantities, in Fig. 3 we show the scaling of structure functions of positive and negative helical components of velocity together with their combinations for the second, fourth, and sixth order. To verify the dimensional scaling predictions (24) and (25) we calculate the local slopes of $S_p^{E,H}(r)$ and $S_p^{\pm}(r)$:

$$\zeta_p^{E,H}(r) = \frac{d \, \log S_p^{E,H}(r)}{d \, \log r}, \quad \zeta_p^{\pm}(r) = \frac{d \, \log S_p^{\pm}(r)}{d \, \log r}, \tag{29}$$

as shown in the insets of Fig. 3. We then used ESS [30] to obtain a better fit of the relative scaling exponents in the inertial range: $\zeta_p^{E,H}/\zeta_3^{E,H}$. In Fig. 4 we compare the scaling exponents $\zeta_p^{E,H}$ and their dimensional predictions (24) and (25). To derive the absolute value of the scaling exponents out of the ESS scaling we have assumed, $\zeta_3^E = 1$ and $\zeta_3^H = 2$ in agreement with the exact scaling properties (3) and (4). From this figure we can see that the dimensional prediction is well verified, except for the presence of a small anomalous correction for high-order moments.
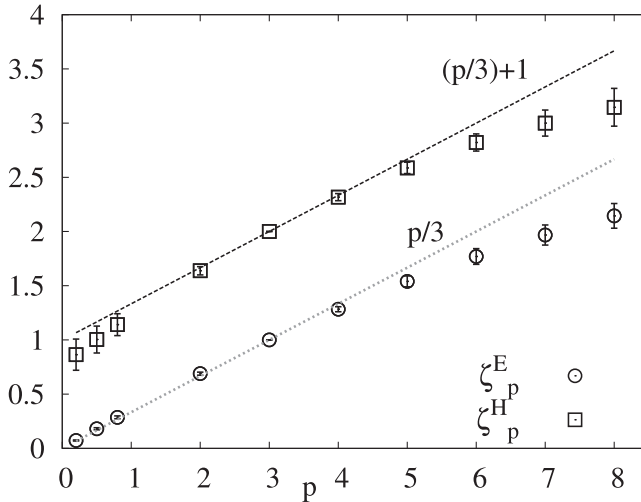

FIG. 4. Scaling exponents $\zeta_p^{E,H}$ of the chiral-symmetric and chiral-antisymmetric structure functions obtained using ESS. The lines with slopes $\frac{p}{3}$ and $\frac{p}{3}+1$ correspond to the dimensional predictions for ζ_p^E and ζ_p^H, respectively. The error bars show the variation of the exponents within the inertial range.
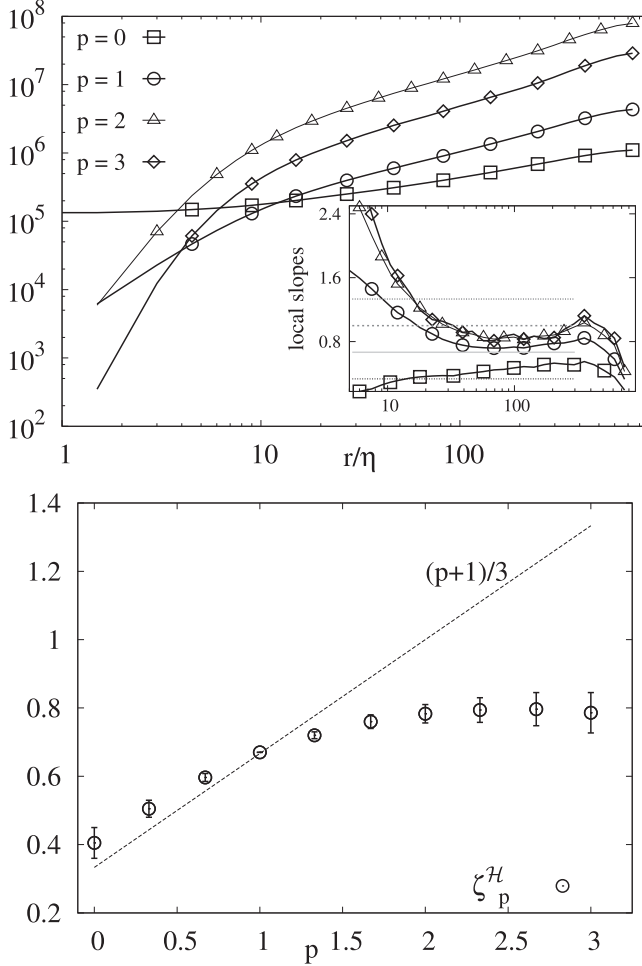
FIG. 5. (Top) Log-log plots of helicity structure functions $\mathcal{H}_p(r)$, defined in (26), for $p = 0$, 1, 2, and 3. Inset: local slopes of the same curves. Horizontal lines indicate the values $\frac{1}{3}$, $\frac{2}{3}$, 1, and $\frac{4}{3}$ from bottom to top. (Bottom) Scaling exponents $\zeta_p^{\mathcal{H}}$ of $\mathcal{H}_p(r)$ obtained using ESS. The line with slope $\frac{p+1}{3}$ corresponds to the dimensional prediction. The error bars show the variation of the exponents within the inertial range.

In Fig. 5 we show the scaling behavior of $\mathcal{H}_p(r)$ for values of p from 0 to 3 compared with the dimensional prediction (28). This works well up to $p \sim 1.5$, while for $p \geqslant 2$ nontrivial anomalous corrections appear. In summary, the scaling exponents for the two sets of helicity-sensitive structure functions $S_p^H(r)$ agree well with the dimensional estimate except for a small anomalous correction which is of the same order of the one observed for the mirror-symmetric terms. One might argue that the two set of anomalous exponents should be correlated, being connected to the dependency on the energy dissipation on the right-hand side of (24) and (25). It is important to notice that helicity is not positive definite, and its dissipation can be split in two different channels, one for positive and one for negative helical components. The theoretical dependency on the Reynolds number of the two processes and of the total helicity dissipation is discussed in Refs. [7,29,31]. Further studies of changing Reynolds number would be needed to clarify the existence of a dissipative anomaly for the helicity cascade and the dependency of the whole statistics on the turbulence intensity. The multiscale nature of the correlation involving vorticity and velocity in $\mathcal{H}_p(r)$ might be particularly

TABLE II. Helicity indices s_i in (30) for the four helical shell models.

Model	s_1	s_2	s_3	s_4	s_5	s_6
No. 1	+	−	−	−	−	+
No. 2	−	−	+	−	+	−
No. 3	−	+	−	+	−	−
No. 4	+	+	+	+	+	+

sensitive to fluctuations of the dissipative physics, hence explaining the large intermittent correction shown in Fig. 5.

In order to investigate further the statistics of the helicity transfer we present in the next section a study of helical shell models, where it is possible to considerably increase the Reynolds number.

IV. HELICAL SHELL MODELS

To check the robustness of the previous findings, we studied the same helical structure functions in a family of helical shell models [23]. Shell models have been useful to study cascade processes and scaling behaviors in turbulent flows since they allow us to achieve very high Reynolds numbers in numerical simulations [22,31–36].

Shell models are based on a simplified dynamical evolution of the energy and helicity transfer by keeping only one (or a few) modes for each spherical shell in Fourier space. They represent a drastic nonexact reduction of the degrees of freedom of the NSE. The original idea is to describe the evolution of a single complex variable u_n, representing all the modes in a shell of wave numbers $k \in [k_n, k_{n+1}]$, with k_n equispaced in logarithmic scale, $k_n = 2^n k_0$. The first step to have a realistic helical structure was done in Ref. [23], where two complex variables u_n^+ and u_n^- carrying positive or negative helicity were introduced for every wave number. This lead to four independent classes of helical shell models, mimicking exactly the four classes of helical interactions of the original NSE [27]. Other models based on similar decompositions have also been proposed [18,37,38]. Here we follow the structure given in [23], where the four possible models have the general form

$$\dot{u}_n^+ = i\left(ak_{n+1}u_{n+2}^{s_1}u_{n+1}^{s_2*} + bk_nu_{n+1}^{s_3}u_{n-1}^{s_4*} + ck_{n-1}u_{n-1}^{s_5}u_{n-2}^{s_6}\right) + f_n^+ - \nu k_n^2 u_n^+,$$

$$\dot{u}_n^- = i\left(ak_{n+1}u_{n+2}^{-s_1}u_{n+1}^{-s_2*} + bk_nu_{n+1}^{-s_3}u_{n-1}^{-s_4*} + ck_{n-1}u_{n-1}^{-s_5}u_{n-2}^{-s_6}\right) + f_n^- - \nu k_n^2 u_n^-. \tag{30}$$

The helicity indices $s_i = \pm$ are reported in Table II, and the coefficients a, b, and c can be found in Table III.

The four classes of interactions conserve energy and helicity separately, as in the original NSE, provided that the coefficients a, b, and c are chosen appropriately. The added value with respect to simpler shell models is that the energy and helicity now have structures similar to (6) and (7) for the

TABLE III. Coefficients of Eqs. (30) for the four helical shell models. These values depend on the shell-to-shell ratio $\lambda = k_n/k_{n-1}$; here $\lambda = 2$. These coefficients guarantee energy and helicity conservation. Conventionally, and without loss of generality, we always choose $a = 1$.

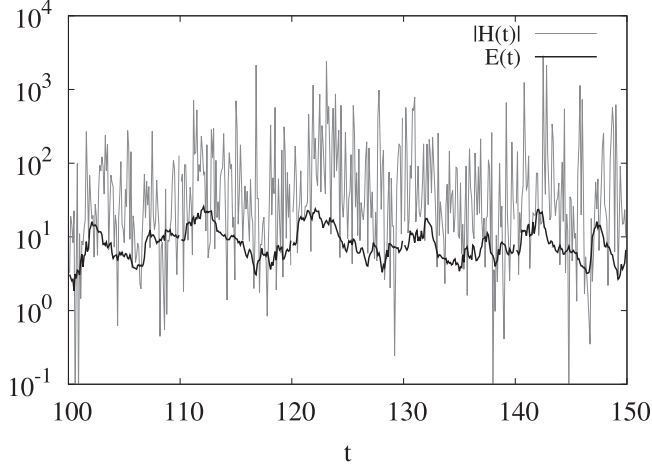| Model	b	c
No. 1	−1/2	1/2
No. 2	−5/2	−3/2
No. 3	−5/6	1/6
No. 4	−3/2	−1/2

FIG. 6. Time evolution of total energy (31) and total helicity (32) in a typical run of the shell model simulation.

NSE [27]:

$$E = E^+ + E^- = \sum_{n=0}^{N} (|u_n^+|^2 + |u_n^-|^2), \tag{31}$$

$$H = H^+ + H^- = \sum_{n=0}^{N} k_n (|u_n^+|^2 - |u_n^-|^2). \tag{32}$$

Here we consider only model no. 3 because its dynamics is known to be dominated by a forward energy cascade, with scaling properties very similar to those of the original NSE [7,23]. The equations that we integrate are the following:

$$\dot{u}_n^+ = i(ak_{n+1}u_{n+2}^- u_{n+1}^{+*} + bk_n u_{n+1}^- u_{n-1}^{+*} + ck_{n-1}u_{n-1}^- u_{n-2}^-) - \nu k_n^2 u_n^+ + f_n^+,$$
$$\dot{u}_n^- = i(ak_{n+1}u_{n+2}^+ u_{n+1}^{-*} + bk_n u_{n+1}^+ u_{n-1}^{-*} + ck_{n-1}u_{n-1}^+ u_{n-2}^+) - \nu k_n^2 u_n^- + f_n^-. \tag{33}$$

We used a fully helical forcing, injecting energy only on the positive modes of the first two shells: $f_0^+ = \xi_{r,0} + i\xi_{i,0}$, $f_1^+ = 0.5(\xi_{r,1} + i\xi_{i,1})$ (where all ξ are Gaussian random variables with $\langle\xi\rangle = 0$ and $\langle\xi^2\rangle = 1$), in order to mimic the setup of the previous section. The number of shells is $N = 25$, $k_0 = 1$, the shell-to-shell ratio is $\lambda = k_n/k_{n-1} = 2$, and the viscosity is $\nu = 1.5 \times 10^{-7}$. The time integration is given by a second order Adams-Bashforth scheme, with explicit integration of the viscous term [39]. With this setup, the Reynolds number is Re $\sim 10^7$, and the large-scale eddy turnover time is $\tau_0 \sim 1$. We let the system evolve for a total time $\sim 10^5 \tau_0$. In Fig. 6 we show the typical evolution of the total energy and of the total helicity in one simulation.

In full analogy with the definitions used in Sec. II for NSE, we can write mirror-symmetric and mirror-antisymmetric structure functions as

$$\mathcal{S}_p^E(k_n) = \langle|u_n^+|^p\rangle + \langle|u_n^-|^p\rangle \sim k_n^{-\zeta_p^E}, \tag{34}$$

$$\mathcal{S}_p^H(k_n) = \langle|u_n^+|^p\rangle - \langle|u_n^-|^p\rangle \sim k_n^{-\zeta_p^H}. \tag{35}$$
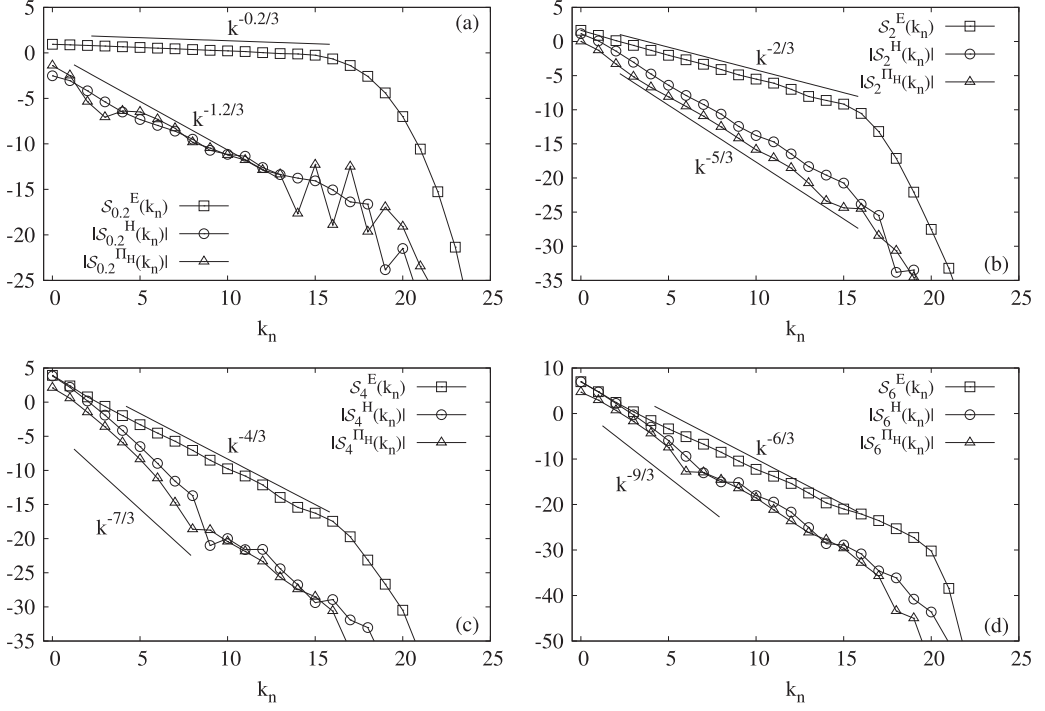
FIG. 7. Log-log (base 2) plots of the symmetric and antisymmetric (35) and (36) structure functions of different orders $p = 0.2$ (a), $p = 2$ (b), $p = 4$ (c), $p = 6$ (d). Straight lines correspond to the predictions (42) and (43).

Additionally, we can define mirror-antisymmetric structure functions based on the third order correlation function responsible for the helicity flux [29,40]:

$$\mathcal{S}_p^{\Pi_H}(k_n) = \left\langle \operatorname{sign}\left(\Pi_n^H\right) \left|k_n^{-2} \, \Pi_n^H\right|^{p/3} \right\rangle \sim k_n^{-\zeta_p^{\Pi_H}}, \tag{36}$$

where for shell model (33) the instantaneous helicity flux at shell n is

$$\Pi_n^H = \sum_{i=0}^{n} \dot{H}_i = \left(\frac{a}{\lambda} + b\right)\delta_n^H + \frac{a}{\lambda}\delta_{n+1}^H, \tag{37}$$

where $\delta_n^H = -2k_n^2(C_{3,n}^+ - C_{3,n}^-)$ with $C_{3,n}^\pm = \operatorname{Im}(u_{n+1}^\mp u_n^{\pm*} u_{n-1}^{\pm*})$. Also for shell models it is possible to use a dimensional argument to predict the scaling of mirror-symmetric and mirror-antisymmetric quantities. Let us consider the energy and helicity balance equations in the inertial range, where dissipative effects are negligible:

$$\varepsilon = \left\langle \Pi_n^E \right\rangle, \quad h = \left\langle \Pi_n^H \right\rangle, \tag{38}$$

where ε and h are the energy and helicity input at large scales, respectively. The instantaneous energy flux at shell n is

$$\Pi_n^E = \sum_{i=0}^{n} \dot{E}_i = (a + b)\delta_n^E + a\delta_{n+1}^E, \tag{39}$$

where $\delta_n^E = -2k_n(C_{3,n}^+ + C_{3,n}^-)$, while the helicity flux is defined in (37). As a consequence,

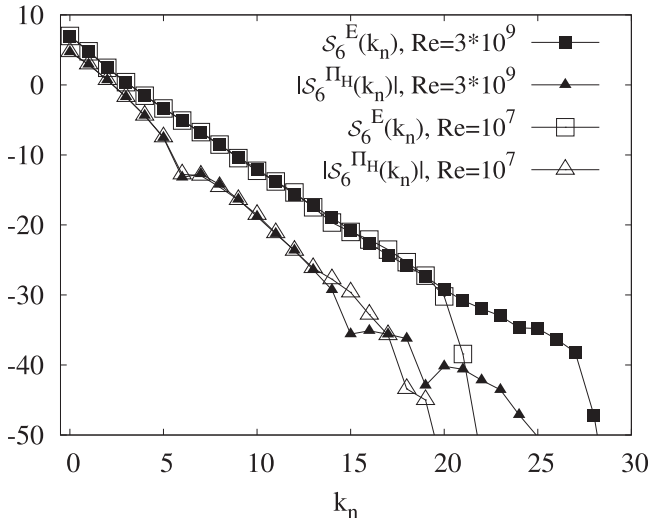$$\langle C_{3,n}^\pm \rangle \sim \varepsilon k_n^{-1} \pm h k_n^{-2}. \tag{40}$$

FIG. 8. Log-log (base 2) plot of the sixth order structure functions for two simulations at different Reynolds numbers: Re $\sim 10^7$ and Re $\sim 3 \times 10^9$.

We can then identify

$$\langle |u_n^\pm| \rangle \sim \langle |C_{3,n}^\pm|^{1/3} \rangle. \tag{41}$$

Substituting (41) in (34) and (35) and considering that (36) should have the same chirality and dimensions of (35), we get the predictions

$$\mathcal{S}_p^E(k_n) \sim k_n^{-p/3}, \tag{42}$$

$$\mathcal{S}_p^H(k_n) \sim \mathcal{S}_p^{\Pi_H}(k_n) \sim k_n^{-(p/3+1)}. \tag{43}$$

In Fig. 7 we show the scaling observed for $\mathcal{S}_p^E(k_n)$, $\mathcal{S}_p^H(k_n)$ and $\mathcal{S}_p^{\Pi_H}(k_n)$ at changing p. The scaling regime for the helical components is deteriorating for higher moments. In particular we observe a change of sign for the antisymmetric structure functions in the middle of the inertial range, hence we plot the absolute values. Spurious contributions to the power law scaling can be a consequence of contaminations coming from the viscous range or from inertial subleading terms. In order to clarify this point, we performed another set of simulations with $N = 31$ shells and Re $\sim 3 \times 10^9$. As can be seen from Fig. 8, even with a longer inertial range, the change of sign and the deterioration in the scaling for high-order helical structure functions are still present, indicating that viscosity might not be the primary cause. In Fig. 9 we summarize the behavior of all scaling exponents, compared with the dimensional predictions (42) and (43). For higher orders, a deviation from the dimensional prediction is observed. As seen in Sec. III for the original NSE, this is possibly due to intermittent corrections or subleading contributions coming from subleading corrections in the helicity flux. Even though the presence of a change of sign in higher-order moments results in large error bars in the estimate of the scaling exponents, our measurements are in good agreement with those reported in Ref. [29]. Our observations disagree with the scaling of subgrid helicity flux measured in DNS of the NSE, reported in Ref. [8]. However, in the latter case, the helicity flux is taken with absolute values, leading to a possible mixing among chiral and mirror-symmetric contributions.

V. CONCLUSIONS

We have studied the statistical properties of helicity in DNS of high Reynolds number flows. We focused on a set of observables sensitive to mirror symmetry, studying the scaling properties
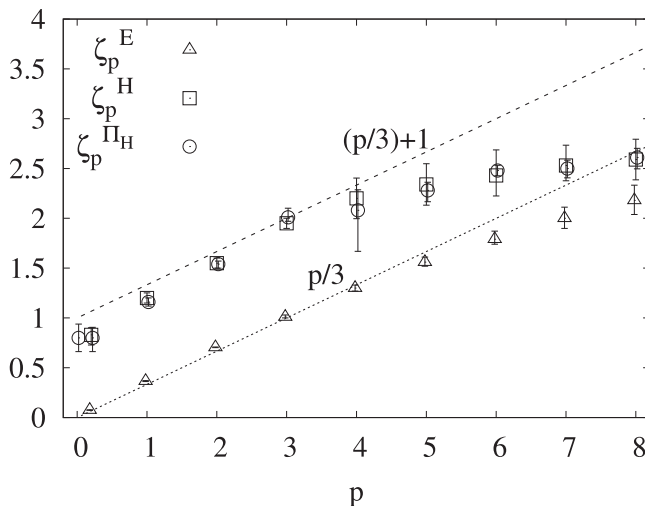
FIG. 9. Exponents of the symmetric and antisymmetric structure functions (34)–(36) as functions of order p. The values are obtained as the mean of linear fits over different ranges of shells. The error bars show the dispersion as a function of the fitting ranges.

of structure functions based on either helical-projected velocity fields or on velocity-vorticity correlations. In both cases we found that chiral contributions are subleading with respect to their counterparts involving only mirror-symmetric components. We investigated the scaling behavior of these subleading corrections in high-order structure functions. A dimensional argument assuming that the main chiral contributions are analytical in the helicity flux captures the power law scaling quite well, except for some anomalous correction. Controlling the multiscale amplitudes of chiral fluctuations is key to develop also subgrid turbulent models for flows that break mirror symmetry either globally or locally [41]. Furthermore, we extended our analysis to higher Reynolds numbers by measuring the statistics of helicity in shell models. Also in shell models we found a scaling behavior quantitatively similar to what reported for the Navier-Stokes equations, including the presence of correction to scaling even at extremely high Reynolds numbers.

---

[1] U. Frisch, *Turbulence: The Legacy of AN Kolmogorov* (Cambridge University Press, Cambridge, UK, 1995).

[2] H. K. Moffatt, The degree of knottedness of tangled vortex lines, J. Fluid Mech. **35**, 117 (1969).

[3] H. K. Moffatt and A. Tsinober, Helicity in laminar and turbulent flow, Annu. Rev. Fluid Mech. **24**, 281 (1992).

[4] A. Brissaud, U. Frisch, J. Leorat, M. Lesieur, and A. Mazure, Helicity cascades in fully developed isotropic turbulence, Phys. Fluids **16**, 1366 (1973).

[5] R. H. Kraichnan and R. Panda, Depression of nonlinearity in decaying isotropic turbulence, Phys. Fluids **31**, 2395 (1988).

[6] H. K. Moffatt, Helicity and singular structures in fluid dynamics, Proc. Nat. Acad. Sci. USA **111**, 3663 (2014).

[7] Q. Chen, S. Chen, and G. L. Eyink, The joint cascade of energy and helicity in three-dimensional turbulence, Phys. Fluids **15**, 361 (2003).

[8] Q. Chen, S. Chen, G. L. Eyink, and D. D. Holm, Intermittency in the Joint Cascade of Energy and Helicity, Phys. Rev. Lett. **90**, 214503 (2003).

[9] P. D. Mininni, A. Alexakis, and A. Pouquet, Scale interactions and scaling laws in rotating flows at moderate Rossby numbers and large Reynolds numbers, Phys. Fluids **21**, 015108 (2009).

[10] E. Deusebio and E. Lindborg, Helicity in the Ekman boundary layer, J. Fluid Mech. **755**, 654 (2014).

[11] E. Herbert, F. Daviaud, B. Dubrulle, S. Nazarenko, and A. Naso, Dual non-Kolmogorov cascades in a von Kármán flow, Europhys. Lett. **100**, 44003 (2012).

[12] L. Biferale, S. Musacchio, and F. Toschi, Inverse Energy Cascade in Three-Dimensional Isotropic Turbulence, Phys. Rev. Lett. **108**, 164501 (2012).

[13] L. Biferale, S. Musacchio, and F. Toschi, Split energy–helicity cascades in three-dimensional homogeneous and isotropic turbulence, J. Fluid Mech. **730**, 309 (2013).

[14] G. Sahoo, F. Bonaccorso, and L. Biferale, Role of helicity for large- and small-scale turbulent fluctuations, Phys. Rev. E **92**, 051002 (2015).

[15] G. Sahoo and L. Biferale, Disentangling the triadic interactions in Navier-Stokes equations, Eur. Phys. J. E **38**, 1 (2015).

[16] T. Gomez, H. Politano, and A. Pouquet, Exact relationship for third-order structure functions in helical flows, Phys. Rev. E **61**, 5321 (2000).

[17] S. Kurien, M. A. Taylor, and T. Matsumoto, Isotropic third-order statistics in turbulence with helicity: The 2/15-law, J. Fluid Mech. **515**, 87 (2004).

[18] E. B. Gledzer and O. G. Chkhetiani, Inverse energy cascade in developed turbulence at the breaking of the symmetry of helical modes, JETP Lett. **102**, 465 (2015).

[19] S. Kurien, M. A. Taylor, and T. Matsumoto, Cascade time scales for energy and helicity in homogeneous isotropic turbulence, Phys. Rev. E **69**, 066313 (2004).

[20] P. D. Mininni and A. Pouquet, Rotating helical turbulence. ii. intermittency, scale invariance, and structures, Phys. Fluids **22**, 035106 (2010).

[21] S. I. Vainshtein, Y. Du, and K. R. Sreenivasan, Sign-singular measure and its association with turbulent scalings, Phys. Rev. E **49**, R2521(R) (1994).

[22] L. Biferale, Shell models of energy cascade in turbulence, Annu. Rev. Fluid Mech. **35**, 441 (2003).

[23] R. Benzi, L. Biferale, R. M. Kerr, and E. Trovatore, Helical shell models for three-dimensional turbulence, Phys. Rev. E **53**, 3541 (1996).

[24] O. G. Chkhetiani, On the third moments in helical turbulence, J. Exp. Theor. Phys. Lett. **63**, 808 (1996).

[25] R. H. Kraichnan, Inertial-range transfer in two-and three-dimensional turbulence, J. Fluid Mech. **47**, 525 (1971).

[26] P. Constantin and A. Majda, The Beltrami spectrum for incompressible fluid flows, Commun. Math. Phys. **115**, 435 (1988).

[27] F. Waleffe, The nature of triad interactions in homogeneous turbulence, Phys. Fluids A **4**, 350 (1992).

[28] Notice that in Ref. [20] these structure functions are defined without the sign, hence are helicity-sensitive only for odd moments.

[29] P. D. Ditlevsen and P. Giuliani, Anomalous scaling in a shell model of helical turbulence, Phys. A **280**, 69 (2000).

[30] R. Benzi, S. Ciliberto, R. Tripiccione, C. Baudet, F. Massaioli, and S. Succi, Extended self-similarity in turbulent flows, Phys. Rev. E **48**, R29 (1993).

[31] P. D. Ditlevsen, *Turbulence and Shell Models* (Cambridge University Press, Cambridge, UK, 2010).

[32] T. Bohr, M. H. Jensen, G. Paladin, and A. Vulpiani, *Dynamical Systems Approach to Turbulence* (Cambridge University Press, Cambridge, UK, 2005).

[33] V. S. L'vov, E. Podivilov, A. Pomyalov, I. Procaccia, and D. Vandembroucq, Improved shell model of turbulence, Phys. Rev. E **58**, 1811 (1998).

[34] P. D. Ditlevsen, Cascades of energy and helicity in the goy shell model of turbulence, Phys. Fluids **9**, 1482 (1997).

[35] S. S. Ray, D. Mitra, and R. Pandit, The universality of dynamic multiscaling in homogeneous, isotropic Navier-Stokes and passive-scalar turbulence, New J. Phys. **10**, 033003 (2008).

[36] R. Stepanov, E. Golbraikh, P. Frick, and A. Shestakov, Hindered Energy Cascade in Highly Helical Isotropic Turbulence, Phys. Rev. Lett. **115**, 234501 (2015).

[37] F. Plunian, R. Stepanov, and P. Frick, Shell models of magnetohydrodynamic turbulence, Phys. Rep. **523**, 1 (2013).

[38] N. M. Rathmann and P. D. Ditlevsen, Role of helicity in triad interactions in three-dimensional turbulence investigated by a new shell model, Phys. Rev. E **94**, 033115 (2016).

[39] M. De Pietro, L. Biferale, and A. A. Mailybaev, Inverse energy cascade in nonlocal helical shell models of turbulence, Phys. Rev. E **92**, 043021 (2015).

[40] L. Biferale, D. Pierotti, and F. Toschi, Helicity transfer in turbulent models, Phys. Rev. E **57**, R2515(R) (1998).

[41] C. Yu, Z. Xiao, Y. Shi, and S. Chen, Joint-constraint model for large-eddy simulation of helical turbulence, Phys. Rev. E **89**, 043021 (2014).